DTIC FILE COPY

(4)

AD-A215 463

MICROWAVE LABORATORY REPORT NO. 89-P-6

PHENOMENOLOGICAL LOSS EQUIVALENCE METHOD FOR PLANAR QUASI-TEM TRANSMISSION LINES USING A THIN NORMAL CONDUCTOR OR SUPERCONDUCTOR

TECHNICAL REPORT

HAI-YOUNG LEE AND TATSUO ITOH

DTIC
ELECTE
DEC 0 8 1989
S D
D CS

DECEMBER 1989

OFFICE OF NAVAL RESEARCH GRANT NO. N00014-89-J-1006

THE UNIVERSITY OF TEXAS AT AUSTIN
DEPARTMENT OF ELECTRICAL ENGINEERING
AUSTIN, TEXAS 78712

DISTRIBUTION STATEMENT A
Approved for public release;
Distribution unlimited

89 12 07 031

MICROWAVE LABORATORY REPORT NO. 89-P-6

PHENOMENOLOGICAL LOSS EQUIVALENCE METHOD FOR PLANAR QUASI-TEM TRANSMISSION LINES USING A THIN NORMAL CONDUCTOR OR SUPERCONDUCTOR

TECHNICAL REPORT

HAI-YOUNG LEE AND TATSUO ITOH

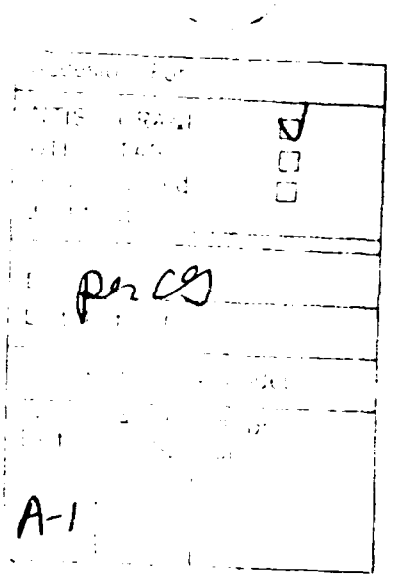

DECEMBER 1989

OFFICE OF NAVAL RESEARCH GRANT NO. N00014-89-J-1006

THE UNIVERSITY OF TEXAS AT AUSTIN
DEPARTMENT OF ELECTRICAL ENGINEERING
AUSTIN, TEXAS 78712

SECURITY CLASSIFICATION OF THIS PAGE (When Data Entered)

REPORT DOCUMENTATION PAGE

READ INSTRUCTIONS BEFORE COMPLETING FORM

1. REPORT NUMBER: Microwave Lab. Report No. 89-P-6
2. GOVT ACCESSION NO.:
3. RECIPIENT'S CATALOG NUMBER:

4. TITLE (and Subtitle): Phenomenological Loss Equivalence Method for Planar Quasi-TEM Transmission Lines Using a Thin Normal Conductor or Superconductor

5. TYPE OF REPORT & PERIOD COVERED: Technical Report

6. PERFORMING ORG. REPORT NUMBER:

7. AUTHOR(s): Hai-Young Lee and Tatsuo Itoh

8. CONTRACT OR GRANT NUMBER(s): Grant No. N00014-89-J-1006

9. PERFORMING ORGANIZATION NAME AND ADDRESS
Dept. of Electrical & Computer Engineering
The University of Texas
Austin, Texas 78712

10. PROGRAM ELEMENT, PROJECT, TASK AREA & WORK UNIT NUMBERS:

11. CONTROLLING OFFICE NAME AND ADDRESS:

12. REPORT DATE: December 1989

13. NUMBER OF PAGES:

14. MONITORING AGENCY NAME & ADDRESS (if different from Controlling Office):

15. SECURITY CLASS. (of this report):

15a. DECLASSIFICATION/DOWNGRADING SCHEDULE:

16. DISTRIBUTION STATEMENT (of this Report):

17. DISTRIBUTION STATEMENT (of the abstract entered in Block 20, if different from Report):

18. SUPPLEMENTARY NOTES:

19. KEY WORDS (Continue on reverse side if necessary and identify by block number)
Conductor Loss, Field Penetration, Superconductor, Quasi-TEM, Loss Equivalence

20. ABSTRACT (Continue on reverse side if necessary and identify by block number)
This technical report presents a simple and practical method for the conductor loss calculation over a wide range of field penetration which can be applied to both normal-state and superconducting transmission lines. The calculated results for microstrip lines and coplanar waveguides using normal conductors and superconductors agree very well with the data obtained using the finite element mehtod, the Monte-Carlo method, and experimental measurements. Because of the calculation simplicity, this method is very suitable for computer-aided design of monolithic microwave and millimeter-wave integrated circuits.

DD FORM 1 JAN 73 1473 EDITION OF 1 NOV 65 IS OBSOLETE
S/N 0102-014-6601

SECURITY CLASSIFICATION OF THIS PAGE (When Data Entered)

PHENOMENOLOGICAL LOSS EQUIVALENCE METHOD FOR PLANAR QUASI-TEM TRANSMISSION LINES USING A THIN NORMAL CONDUCTOR OR SUPERCONDUCTOR

This technical report presents a simple and practical method for the conductor loss calculation over a wide range of field penetration which can be applied to both normal-state and superconducting transmission lines. This phenomenological loss equivalence method is based on the observation of the conduction current distribution as the quasi-static field of a quasi-TEM transmission line penetrates into the conductor.

In this method, a planar quasi-TEM transmission line, having a finite conductor thickness on the order of the penetration depth, is approximated by an equivalent single strip which is assumed to have the same conductor loss as the transmission line. Then, the distributed internal impedance of the transmission line is calculated from the equivalent single strip and all the propagation characteristics are obtained by incorporating the internal impedance into the circuit model of transmission line.

The calculated results for microstrip lines and coplanar waveguides using normal conductors and superconductors agree very well with the data obtained using the finite element method, the Monte-Carlo method, and experimental measurements. Because of the calculation simplicity, this method is very suitable for computer-aided design of monolithic microwave and millimeter-wave integrated circuits.

TABLE OF CONTENTS

Chapter 1

Introduction

High speed and high degrees of integration in modern integrated circuits, especially in monolithic microwave integrated circuits, require very narrow and thin metal interconnection lines. High-speed electro-optic devices, such as traveling-wave optical modulators, use very narrow and thin electrodes for a very wide bandwidth. In the very thin normal conductor line, the field penetration depth, which decreases with increasing frequency due to the skin-effect, can be comparable with the line thickness even at high frequency. Therefore, the field penetration effect should be taken into account for the wideband characterization of the lines. On the other hand, superconductors have very high conductivities and can be used to reduce the conductor losses of the lines with a small cross-section[1]. However, if the thickness or the width of the superconducting line is small enough to let the field penetrate deep into the line, the conductor loss will be increased and the merit of the almost non-dispersive transmission characteristic will be lost.

Therefore, for both small normal-conducting and superconducting lines, the conductor loss must be characterized in a wide field-penetration range by taking the field penetration effect into consideration. DC calculation at complete penetration and the incremental inductance method at shallow penetration[2], however, cannot be used directly in the wide range of field penetration. The DC calculation assumes a uniform

current distribution inside the conductor at the complete field penetration. On the other hand, the incremental inductance method is valid only if the conductor thickness is several times the penetration depth. Therefore, in order to consider the penetration effect, several loss analyses have been carried out for microstrip-like structures. A variational formulation of the penetration-effect problem[3] was used to calculate the conductor loss of a single thin strip which has a rectangular cross section without a substrate and a ground plane. The finite element method was also applied to microstrip-like transmission line structures to calculate the resistance and reactance[4], [5]. However, these methods are not appropriate for computer-aided-design implementation, since they require extensive formulations and numerical computations. A simple modification of the penetration-effect resistance[6] is valid only for a very thin and wide strip.

This technical report presents a simple and practical method for the conductor loss calculation in a wide range of field penetration[7], which can be applied to normal-state[8] and superconducting transmission lines[9]. This phenomenological loss equivalence method(PEM) is based on the observation of the current distribution change as the quasi-static field of a quasi-TEM transmission line penetrates more into the conductor. In this method, a planar quasi-TEM transmission line, having a finite conductor thickness on the order of the penetration depth, is approximated by an equivalent single strip with finite thickness in which current distribution is assumed to be uniform on the strip surface. The width and thickness of the equivalent strip are obtained from the cross-sectional geometry of the original line, while the conducting material is the same as that of the original line. Since the geometry of the equivalent strip obtained is material-independent, it can be used for any normal-state or

superconducting line by substituting the conducting material. Therefore, the distributed internal impedance of the transmission line can be approximately calculated from the equivalent single strip and all the propagation characteristics can be obtained by incorporating the internal impedance into the circuit model of the transmission line.

Chapter 2

Penetration of Electromagnetic Fields into a Good Conductor

2.1. Introduction

A normal-state conductor has the skin depth (δ) which is inversely proportional to the square root of frequency. Then, the field penetrates deeper at lower frequency and the current flowing inside the conductor becomes more uniform. On the other hand, a superconductor has an almost constant penetration depth (λ) at a given temperature below the critical temperature (T_c) and the field penetration remains almost unchanged with the frequency. Based on the two-fluid model[10], a superconductor can be described as a conductor which has the complex conductivity ($\sigma = \sigma_n + j\,\sigma_s$, where σ_n and σ_s are the normal and super-conductivities, respectively) depending on the temperature and the frequency. Therefore, by assuming a generalized complex conductivity ($\sigma = \sigma_r + j\,\sigma_i$), we can treat both the normal and super-conductors with an identical formulation.

At very high frequencies, appreciable deviations from the local conductivity modeling can occur due to so-called anomalous effect[11] in which mean free-path of the normal electrons can become comparable to the penetration depth or the conductor thickness. Therefore, the relation between the conduction current and the electric field will have a non-local form[12] which integrates all the contribution of nearby electrons. This effect exists in both normal conductor and superconductor and results in a large

increase in conductor loss. Although this effect is not included in this phenomenological loss equivalence method, the local conductivity modeling can be used in most of practical situations with a reasonable agreement since the anomalous effect occurs only at very high frequencies.

2.2. Planewave propagation into a good conducting medium

In this section, we consider the field penetration of a plane wave into a conducting medium with finite conductivity as shown in Fig.2.1(a). For a simplification, we assume a normal incidence in infinitely thick conductor. However, in any incidence angle, the field travels almost in normal direction inside the conductor. That is because the wave vector inside a good conductor is very larger than in any dielectric material and hence, the small tangential wave vector of the incident wave does not affect the normal component of the large wave vector inside the conductor. This characteristic can be used very effectively to describe the field penetration effect at a given surface geometry using the surface impedance obtained for the normal planewave incidence.

Electric and magnetic fields inside the conductor can be expressed by Helmholtz equations obtained from Maxwell's equations using time-harmonic convention of $e^{j\omega t}$ as follow.

$$\begin{aligned} (\nabla^2 - j\omega\mu\sigma + \omega^2\mu\varepsilon)\,\underline{E} = 0 \\ (\nabla^2 - j\omega\mu\sigma + \omega^2\mu\varepsilon)\,\underline{H} = 0 \end{aligned} \qquad (2.1)$$

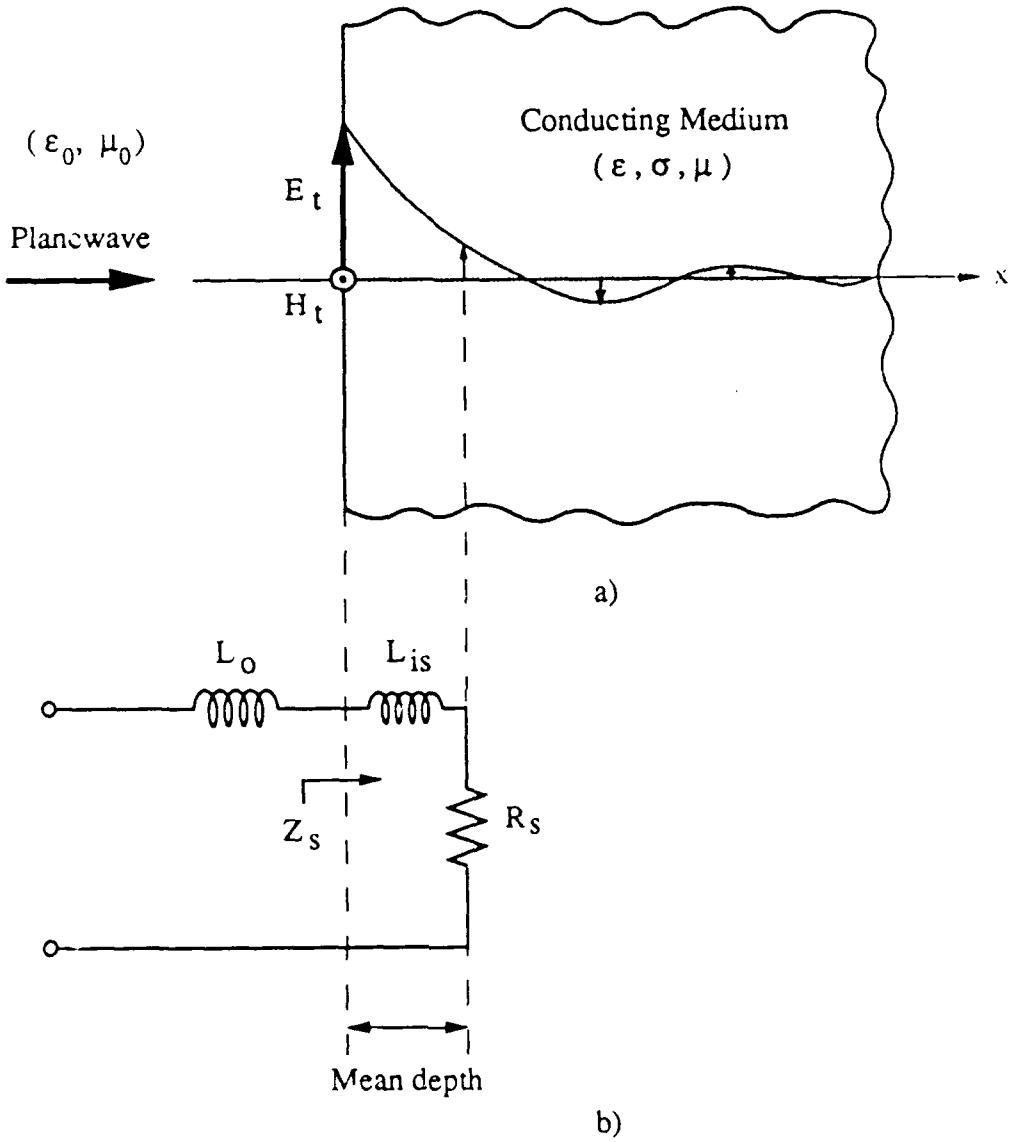

Fig. 2. 1. (a) Penetration of a planewave into a good conductor and (b) the equivalent lumped circuit

where ε, μ, and σ are the permitivity, the permeability, and the conductivity of the conductor. By inserting the phaser notation (e^{-jkx}) of planewave solution into the above Helmholtz equations, we can get the following dispersion relation.

$$k^2 = \omega^2 \mu \varepsilon \left(1 - j \frac{\sigma}{\omega \varepsilon} \right) \tag{2.2}$$

Since conduction current of a good conductor is much larger than the displacement current (i.e. $\sigma >> \omega \varepsilon$), the above dispersion relation can be reduced simply as

$$k = \pm \sqrt{-j \omega \mu \sigma} \tag{2.3}$$

where the positive and negative signs are for the waves traveling positive and negative x directions, respectively. Therefore, the incident fields decay exponentially from the conductor surface due to the imaginary part of k and oscillate due to the real part of k.

The depth of penetration (Δ) is defined by the depth at which the fields (or the conduction current density) is attenuated by $1/e$ from the surface value. Therefore, the depth of penetration can be expressed using the imaginary part of k.

$$\Delta = \frac{1}{-\mathrm{Im}(k)} \tag{2.4}$$

The characteristic impedance of the conducting medium can be obtained from Maxwell's equation and the dispersion relation (2.3) as follows.

$$Z_0 = \pm \frac{\omega \mu}{k} = \sqrt{\frac{j \omega \mu}{\sigma}} \tag{2.5}$$

Now, if we define the surface impedance of a conductor (Z_s) by the ratio of the tangential electric field (E_t) to the magnetic field (H_t) at the conductor surface, the

surface impedance represents the input impedance of the conductor seen at the conductor surface.

$$Z_s = \frac{E_t}{H_t} = Z_{in} \tag{2.6}$$

If the conducting medium is infinitely thick in the propagation direction, the input impedance will be the characteristic impedance of the conductor because there is no reflected wave traveling in negative x direction inside the conductor. Therefore,

$$Z_s = R_s + j\omega L_{is} = \sqrt{\frac{j\omega\mu}{\sigma}} \tag{2.7}$$

The surface impedance consists of the real and imaginary parts, which associates respectively with the ohmic resistance (R_S) and the internal inductance per square area (L_{iS}) due to the field penetration. The ohmic resistance comes from the finite conduction current flowing inside the conductor by the penetrated electric field. The internal magnetic flux inside the conductor results in the internal inductance which is additional to the external inductance (L) due to the magnetic flux outside the conductor. The concept of the internal impedance is illustrated in Fig. 2.1(b) using circuit elements, where resistance and internal inductance, due to the finite conduction current and the magnetic flux penetration, are shown inside the conductor and parallel capacitance representing small displacement current is neglected inside the conductor.

2.2.1. Field penetration into a normal conductor

For a normal-state conductor, the conductivity is pure real and hence, the real and imaginary parts of the surface impedance per square area are the same.

$$Z_s = (1+j)\sqrt{\frac{\omega\mu}{2\sigma}} = \frac{(1+j)}{\sigma\delta}$$
$$\delta = \frac{1}{\sqrt{\pi f \mu \sigma}} \tag{2.8}$$

where the quantity δ, called the skin depth of the normal conductor, has the significance of the penetration depth defined by (2.4). The surface resistance and the internal inductance per square area can be written in terms of the skin depth as follow.

$$R_s = \mathrm{Re}(Z_s) = \frac{1}{\sigma\delta}$$
$$L_{is} = \frac{\mathrm{Im}(Z_s)}{\omega} = \mu\frac{\delta}{2} \tag{2.9}$$

The above equations show that the resistance and the internal inductance are those of layers whose thicknesses are equal to the skin depth and one half of the skin depth, respectively. In other word, the mean depths of the surface resistance and the internal inductance of a normal conductor are respectively the skin depth and one half of that. A significance of the field penetration effects in normal conductors is the skin depth which is inversely proportional to the square root of frequency. Therefore, the penetration effect for finite conductor thickness is significant at low frequencies and the field distribution inside the conductor finally becomes uniform at DC.

2.2.2. Field penetration into a superconductor

Although the conductivity modeling of superconductor, especially for high-T_c superconductors have not been established well, two-fluid model[10] has been used generally below the bandgaps of the superconductors because of its simplicity. Mattis and Bardeen derived a more realistic result for the conductivity using the BCS weak-

coupling theory at frequencies approaching the bandgap frequency[11]. While the Mattis - Bardeen theory describes the conductivity even above the bandgap frequency and can be used for this phenomenological loss equivalence method, the two-fluid model has been used throughout this technical report because of its simplicity and reasonable description of the superconductivity below the bandgap.

The two-fluid model postulates that a fraction of the conduction electrons is in the lowest-energy (or superconducting) state with the remainder in the excited (or normal) state. Using London equation and low frequency assumption[10], the complex conductivity can be expressed as the sum of the contributions from normal current (for the quasi-particles) and supercurrent (for the Cooper pairs) :

$$\sigma = \sigma_n - j\,\sigma_s$$

$$\sigma_n = \sigma_{nn}\left(\frac{T}{T_c}\right)^{\beta}\ ,\ \sigma_s = \frac{1-\left(\frac{T}{T_c}\right)^{\beta}}{\omega\,\mu\,\lambda_0^{\,2}} \qquad (2.10)$$

where σ_{nn}, λ_o, and μ are the normal conductivity at the critical temperature (T_c), the penetration depth at 0 K, and the permeability of the superconductor. Here β is an empirical parameter for a given superconductor such that $1 \le \beta \le 4$. The imaginary part (σ_s) of the conductivity associated with the supercurrent is much larger than the real part (σ_n) associated with the normal current below the critical temperature. Fig. 2.2 shows the heuristic equivalent model of a superconductor which is a parallel connection of a normal resistor and an ideal inductor associated with the normal current and the supercurrents, respectively.

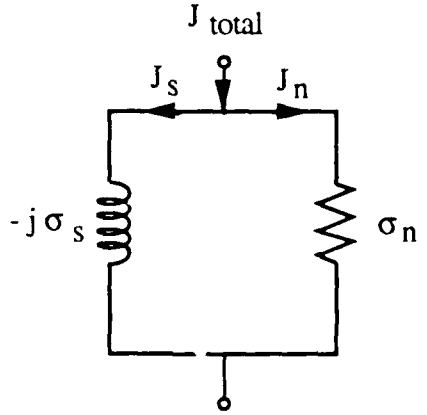

Fig. 2. 2. Equivalent circuit representation of a superconductor in two-fluid model

Since $\sigma_s >> \sigma_n$ for a superconductor below the T_c, the propagation constant (k) in (2.3) is almost pure imaginary and then, the incident fields only decay exponentially from the superconductor surface. The penetration depth (λ) of a superconductor can be approximately calculated below the T_c using (2.4) and (2.10) as follows.

$$\lambda \approx -\frac{1}{\sqrt{\omega \mu \sigma_s}} = \frac{\lambda_0}{\sqrt{1 - \left(\frac{T}{T_c}\right)^{\beta}}} \qquad (2.11)$$

The penetration depth is almost constant with the frequency and only depends on the temperature for a given superconductor. That is because the dominant supercurrent is inversely proportional to the frequency of the fields and hence, the complex propagation constant in dispersion relation (2.3) is almost frequency-independent. This is a very important characteristic of superconductors as well as their high supercurrent.

The surface impedance of a superconductor can be obtained using (2.7) and (2.10) as follows.

$$Z_s \approx \frac{1}{\lambda\left(\frac{\sigma_n}{2} - j\,\sigma_s\right)} = \frac{\left(\frac{\sigma_n}{2} + j\,\sigma_s\right)}{\lambda\,\sigma_s^{\,2}} \tag{2.12}$$

$$R_s = \mathrm{Re}\,(Z_s) = \frac{\sigma_n}{2\,\lambda\,\sigma_s^{\,2}} \tag{2.13}$$

$$L_{is} = \frac{\mathrm{Im}\,(Z_s)}{\omega} = \mu\,\lambda \tag{2.14}$$

The ohmic resistance is very small below the T_c and the mean depth of the internal inductance is the penetration depth (λ) while the mean depth of a normal conductor is one half of the skin depth ($\delta/2$). Since superconductors have very small penetration depths which are only temperature-dependent below the bandgap frequency, the penetration effect is important only for very thin structures or around the critical temperatures.

2.3. Surface impedance of a conducting plane with finite thickness

If the conducting plane has finite thickness, the fields inside the conductor will be reflected back and forth between the two conductor surfaces. As mentioned in the previous sections, the field inside the conductor propagates in the normal direction of the conductor surface for any incidence angle. Therefore, the conducting plane behaves as a highly lossy transmission line terminated by the air on both ends in the normal

direction. Since good conductors have much smaller characteristic impedance than the air as shown in (2.5), we can assume the both ends of the transmission line are open. Therefore, the surface impedance of a conducting plane with finite thickness (t) can be expressed using a formula for transmission line as

$$Z_s^t = R_s^t + j\,\omega\,L_i^t = Z_s \coth(-jkt)$$

$$= \sqrt{\frac{j\omega\mu}{\sigma}} \coth\left[(1+j)\sqrt{\frac{\omega\mu\sigma}{2}}\,t\right] \qquad (2.15)$$

The last coth term of the surface impedance shows a correction factor for the finite thickness due to the multiple reflections between the conductor surfaces. The surface impedance can be used for any incidence angle because of the normal propagation of the field inside the conductor. Therefore, if the field distribution on the conductor surface is obtained by assuming the perfect conductor, each surface of the conductor can be approximately replaced by the corresponding surface impedance. Then, the imperfect conductor effect, such as the conductor loss, can be readily calculated. The conductor thickness is not necessarily infinite if we use the surface impedance (2.15) for finite conductor thickness. This can be used effectively to characterize conducting planes with finite thickness comparable to the penetration depth. For a normal conductor, this effect is significant at low frequencies because the skin depth increases with decreasing frequency. Since superconductors have very shallow penetration depths below the critical temperatures, this effect takes place normally in very thin and narrow superconductors.

Chapter 3

Incremental Inductance Rule and Geometric Factor

3.1. Introduction

As discussed in previous chapters, the field penetration into an imperfect normal conductor or superconductor results in finite surface resistance and internal inductance. The surface resistance dissipates the field energy through the ohmic loss and the small internal inductance is added to the external inductance of the perfectly conducting structure. Now, the total internal impedance (Z_i) of a given structure, due to the field penetration, can be obtained by summing up all the contribution of the internal impedance coming from the entire exposed conductor surface. The total internal impedance can be calculated using so-called incremental inductance rule[2] which calculates the internal inductance by the increment of the total inductance caused by the penetration of the magnetic flux. The incremental inductance rule is entirely based on inductance calculation and valid essentially if the penetration depth is very shallow compared to the conductor thickness and radius of curvature. By the way, this rule can be modified for deep penetration if we use the surface impedance defined in (2.15) for finite conductor thickness.

In the shallow penetration, the total internal impedance can be expressed using the surface impedance and the geometric factor which depend only on the material properties and the surface geometry, respectively. Therefore, a given structure can be

substituted by any conducting surface which has the same geometric factor and the same material properties. This idea has been used very effectively in phenomenological loss equivalence method, to be discussed in next chapter, where a given conductor geometry is effectively represented by a single equivalent strip.

3.2. Incremental inductance rule

The internal inductance is caused by the penetration of the magnetic flux into the conductor. This internal magnetic flux has the mean depths of $\delta/2$ and λ for normal conductors and superconductors, respectively, as shown in (2.9) and (2.14). Therefore, the internal inductance (L_{is}) is equivalent to the increment of the external inductance caused by receding the conductor surface to the mean depth as shown below.

$$L_{is} = \left(\frac{\partial L}{\partial n}\right)\frac{\delta}{2} \qquad \text{for normal conductors} \qquad (3.1)$$

$$= \left(\frac{\partial L}{\partial n}\right)\lambda \qquad \text{for superconductors} \qquad (3.2)$$

where n is the normal recession of the conductor surface. The internal reactance ($j\omega L_{is}$) is related to the internal resistance (R_s) by the surface impedance given in (2.7). Therefore, the internal impedance of a conductor surface can be expressed using the surface impedance (Z_s) and the increment of the external impedance ($\partial L/\partial n$) on the conductor surface. Finally, the total internal impedance (Z_i) can be obtained by summing up all the internal impedance on each exposed conductor surface as follows.

$$Z_i = R + j\,\omega\, L_i \approx \sum_m \frac{1}{\mu_m}\left(\frac{\partial L}{\partial n_m}\right) Z_{sm} \qquad (3.3)$$

3.3. Concept of the geometric factor

If each conductor surface has the same surface impedance, the above total internal impedance can be expressed using the surface impedance and the geometric factor G shown below.

$$Z_i = \frac{1}{\mu} \sum_m \left(\frac{\partial L}{\partial n_m} \right) Z_s = G \; Z_s \tag{3.4}$$

$$G \equiv \frac{1}{\mu} \sum_m \left(\frac{\partial L}{\partial n_m} \right) \tag{3.5}$$

where G is defined as a geometric factor because it can be obtained only from the conductor geometry. This implies that a given structure has a unique geometric factor and different structures having the same geometric factor can be said equivalent to each other in terms of internal impedance at shallow penetration. This implication is very important for the phenomenological loss equivalent method to be explained in next chapter.

Since the external magnetic flux is proportional to the surface current density, the increment of the external inductance is associated with the distribution of current density on each conductor surface. For instance, if the current density is higher on a surface, the increment of the external inductance will be higher on the surface. Therefore, the geometric factor G represents the surface current distribution of a given geometry. If the surface current concentrates more in a small surface area, the increment of the external inductance on the surface (or G) will be higher and then, the internal impedance and the conductor loss will be increased. Therefore, in order to

reduce the conductor loss, we should spread out the surface current equally on the entire conductor surface and hence, decrease the geometric factor.

3.4. Calculation of the geometric factor for quasi-TEM lines

The geometric factor of a structure can be obtained readily if we know the external inductance for perfect conductor case using full-wave analyses or empirical formulas. For quasi-TEM transmission lines, such as a microstrip, a coplanar waveguide, and a coplanar strip, the geometric factors can be calculated using quasi-static surface current distributions on the cross-sectional surfaces of the lines. If empirical formulas of the effective index and the characteristic impedance are given for a quasi-TEM transmission line, the geometric factor can be readily calculated by obtaining the derivative of the external inductance as shown in (3.5).

In many publications[13],[14], the incremental inductance method has been applied to the quasi-TEM lines to obtain the conductor losses based on several empirical formulas. However, their published expressions for the conductor losses are not consistent and, moreover, some expressions are based on inaccurate formulas or seem to have typographical errors. Therefore, in order to obtain more accurate and reliable geometric factors for typical quasi-TEM lines, the geometric factors are derived based on their empirical formulas currently available and very accurate in the given ranges.

3.4.1. Geometric factor of a microstrip line

For the microstrip line with finite strip thickness shown in Fig. 3.1, simple and accurate closed form expressions of the effective index (ε_{reff}) and the characteristic impedance (Z_0) are empirically obtained for the case of ideal conductor[15]. Although

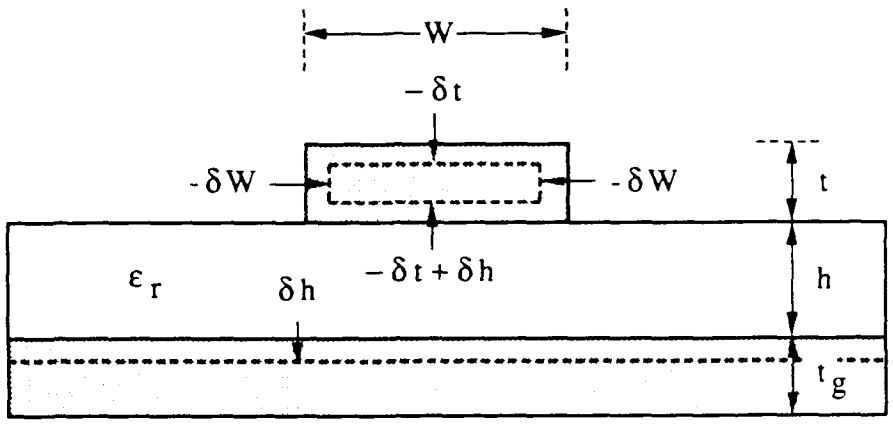

Fig. 3. 1. Recession of conducting walls of a microstrip line for the calculation of the geometric factor

the expressions do not describe the dispersion, the expressions are the most accurate formulas current available in a wide range of aspect ratio ($0.1 \le W/h \le 20$) and strip thickness ($t/h \le 0.2$). The dispersion also can be incorporated into the quasi-TEM expressions using empirical dispersion equations[16]. The formulas are shown below and used to calculate the geometric factor.

$$Z_0 = \begin{cases} \dfrac{60}{\sqrt{\varepsilon_{reff}}} \ln\left(\dfrac{8}{W/h} + 0.25\dfrac{W_e}{h}\right) & , W/h \le 1 \\ \dfrac{120\pi}{\sqrt{\varepsilon_{reff}}}\left[\dfrac{W_e}{h} + 1.393 + 0.667\ln\left(\dfrac{W_e}{h} + 1.444\right)\right]^{-1} & , W/h \ge 1 \end{cases} \tag{3.6}$$

where

$$\frac{W_e}{h} = \begin{cases} \frac{W}{h} + \frac{1.25}{\pi}\frac{t}{h}\left(1 + \ln\frac{4\pi W}{t}\right), & W/h \le \frac{1}{2\pi} \\ \frac{W}{h} + \frac{1.25}{\pi}\frac{t}{h}\left(1 + \ln\frac{2h}{t}\right), & W/h \ge \frac{1}{2\pi} \end{cases} \tag{3.7}$$

and

$$\varepsilon_{reff} = \begin{cases} \frac{\varepsilon_r + 1}{2} + \frac{\varepsilon_r - 1}{2}\left[\left(1 + \frac{12}{W/h}\right)^{-1/2} + 0.04\left(1 - \frac{W}{h}\right)^2\right] - C, & W/h \le 1 \\ \frac{\varepsilon_r + 1}{2} + \frac{\varepsilon_r - 1}{2}\left(1 + \frac{12}{W/h}\right)^{-1/2} - C, & W/h \ge 1 \end{cases} \tag{3.8}$$

in which

$$C = \frac{\varepsilon_r - 1}{4.6}\frac{t/h}{\sqrt{W/h}}$$

The above formulas can be transformed into formulas of the distributed capacitance (C) and external inductance (L_o). The distributed external inductance has been obtained using the characteristic impedance of the microstrip with substrate filled with air (Z_0^a) and the free-space light velocity (c) since the dielectric substrate does not affect the external magnetic flux and hence, the external inductance. Therefore,

$$L_0 = \frac{Z_0^a}{c} \tag{3.9}$$

The geometric factor has been calculated by summing up all the incremental inductances coming from the recession of all conducting walls shown in Fig. 3.1. For a simplification we assumed the same conductor for the strip and the ground plane.

The geometric factor shown below has been obtained from the derivative of the external inductance and some algebraic manipulations.

$$G = \frac{1}{\mu}\sum_{m}\left(\frac{\partial L}{\partial n_m}\right) = \frac{1}{\mu}\left[\left(\frac{\partial L}{\partial h} - 2\frac{\partial L}{\partial W} - 2\frac{\partial L}{\partial t}\right)_{strip} + \left(\frac{\partial L}{\partial h}\right)_{\substack{ground\\plane}}\right] \tag{3.10}$$

$$= \begin{cases} \dfrac{1}{\pi}\dfrac{A}{h}\left[\dfrac{32 - \left(\dfrac{W_e}{h}\right)^2}{32 + \left(\dfrac{W_e}{h}\right)^2}\right], & W/h \le 1 \\ 2\,\varepsilon_{reff}\left(\dfrac{Z_0}{120\,\pi}\right)^2 \dfrac{A}{h}\left[\dfrac{W_e}{h} + \dfrac{0.667\dfrac{W_e}{h}}{\left(\dfrac{W_e}{h} + 1.444\right)}\right], & W/h \ge 1 \end{cases} \tag{3.11}$$

where

$$A = \begin{cases} 1 + \dfrac{h}{W_e}\left[1 + \dfrac{1.25}{\pi}\left(\ln\dfrac{4\pi W}{t} + \dfrac{t}{W}\right)\right], & W/h \le \dfrac{1}{2\pi} \\ 1 + \dfrac{h}{W_e}\left[1 + \dfrac{1.25}{\pi}\left(\ln\dfrac{2h}{t} - \dfrac{t}{h}\right)\right], & W/h \ge \dfrac{1}{2\pi} \end{cases}$$

3.4.2. Geometric factor of a coplanar waveguide

For the coplanar waveguide shown in Fig.3.2, quasi-static analysis using conformal mapping[17] has been usually used to obtain the closed form expressions of the effective index and the characteristic impedance. The analysis holds only for infinite substrates and infinitesimally thin conductors. A correction for the finite conductor thickness[14] has been carried out based on the concept of increase in

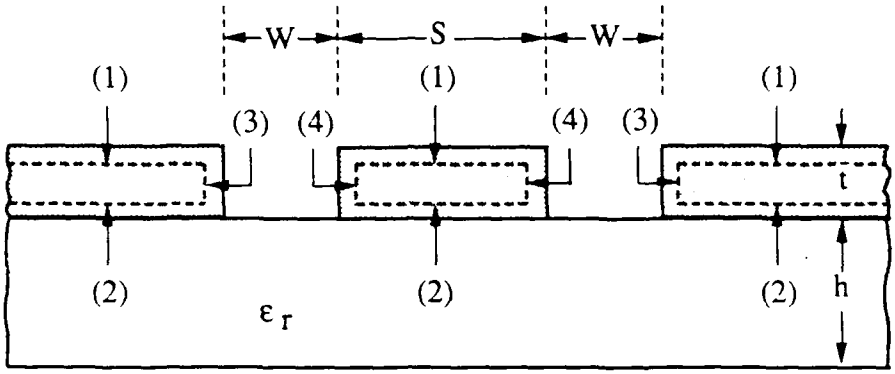

$$(1) = -\delta t$$
$$(2) = -\delta t + \delta h$$
$$(3) = \delta W$$
$$(4) = \delta W - \delta(2S)$$

Fig. 3. 2. Recession of conducting walls of a coplanar waveguide for the calculation of the geometric factor

microstrip width due to the finite thickness shown in (3.7). Effect of the finite substrate thickness is also included in the following closed form expression of the effective index[14] by curve-fitting numerical results[18]. The conformal mapping result and the corrections are summarized in the following expressions of the effective index and the characteristic impedance.

$$Z_0 = \frac{30\pi}{\sqrt{\varepsilon_{reff}}} \frac{K'(k_e)}{K(k_e)} \tag{3.12}$$

$$\varepsilon_{reff} = \varepsilon_{re} - (\varepsilon_{re} - 1)\frac{0.7\,\frac{t}{W}}{\left[\frac{K(k)}{K'(k)} + 0.7\,\frac{t}{W}\right]} \tag{3.13}$$

where

$$\varepsilon_{re} = \frac{\varepsilon_r + 1}{2}\left\{ \tanh\left[1.785 \log\left(\frac{h}{W}\right) + 1.75\right] + \frac{k\,W}{h}\left[0.04 - 0.7\,k + 0.01\left(1 - 0.1\,\varepsilon_r\right)(0.25 + k)\right]\right\} \tag{3.14}$$

$$k = \frac{S}{S + 2W}\ ,\ k_e = \frac{S_e}{S_e + 2W'_e}$$

$$S_e = S + \Delta\ ,\ W_e = W - \Delta$$

$$\Delta = \frac{1.25\,t}{\pi}\left[1 + \ln\left(\frac{4\pi\,S}{t}\right)\right]$$

, and $K(k)$ and $K'(k)\left[= K\left(\sqrt{1 - k^2}\right)\right]$ are the complete elliptic integral of the first kind and that with complementary modular, respectively.

Now, the geometric factor can be obtained in the same way as that of the microstrip mentioned in previous section. In order to calculate the derivative of the external inductance, the ratio of the elliptic integrals (K'/K) is expressed by simple algebraic formulas[19]. The recession of conducting walls are shown in Fig. 3.2 and added to calculate the following geometric factor.

$$G = \frac{1}{\mu}\left[\left(-\frac{\partial L}{\partial t} + \frac{\partial L}{\partial h}\right)_{(1)} + \left(-\frac{\partial L}{\partial t}\right)_{(2)} + \left(\frac{\partial L}{\partial W}\right)_{(3)} + \left(\frac{\partial L}{\partial W} - 2\,\frac{\partial L}{\partial S}\right)_{(4)}\right] \tag{3.15}$$

$$= \frac{P}{\pi W}\left(1+\frac{S}{W}\right)\frac{1+\frac{1.25}{\pi}\left[\frac{t}{S}+\ln\frac{4\pi S}{t}\right]}{\left[2+\frac{S}{W}-\frac{1.25\,t}{\pi W}\left(1+\ln\frac{4\pi S}{t}\right)\right]^2} \qquad (3.16)$$

where

$$P = \begin{cases} \dfrac{k_e}{\left(1-\sqrt{1-k_e^2}\right)\left(1-k_e^2\right)^{3/4}}, & 0.0 \le k_e \le 0.707 \\ \dfrac{1}{\left(1-k_e\right)\sqrt{k_e}}\left(\dfrac{K'(k_e)}{K(k_e)}\right)^2, & 0.707 \le k_e \le 1.0 \end{cases}$$

3.4.3. Geometric factor of a coplanar strip

Since coplanar strip and coplanar waveguide configurations are complementary to each other, closed form expressions of effective index and characteristic impedance for the coplanar strip can be obtained by interchanging conducting and air-dielectric walls of the coplanar waveguide. Therefore, following final expressions[14] for the coplanar strip are very similar to those for the coplanar waveguide except interchanges of W and S.

$$Z_0 = \frac{120\,\pi}{\sqrt{\varepsilon_{reff}}}\frac{K(k_e)}{K'(k_e)} \qquad (3.17)$$

$$\varepsilon_{reff} = \varepsilon_{re} - \left(\varepsilon_{re}-1\right)\frac{1.4\,\frac{t}{S}}{\left[\frac{K'(k)}{K(k)}+1.4\,\frac{t}{S}\right]} \qquad (3.18)$$

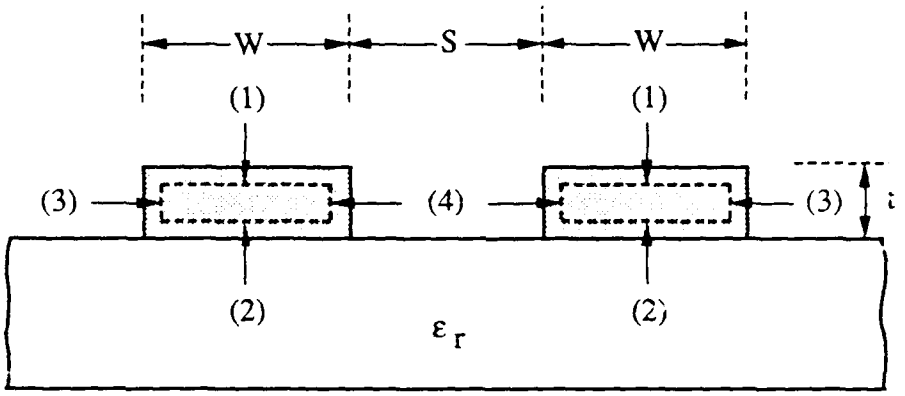

$$(1) = -\delta t$$
$$(2) = -\delta t + \delta h$$
$$(3) = -\delta W$$
$$(4) = -\delta W + \delta(2S)$$

Fig. 3. 3. Recession of conducting walls of a coplanar strip for the calculation of the geometric factor

where

$$S_e = S - \Delta \ , \ W_e = W + \Delta$$

$$\Delta = \frac{1.25\,t}{\pi}\left[1 + \ln\left(\frac{4\pi W}{t}\right)\right]$$

and ε_{re}, k, k_e, K, and K' are shown in previous section for coplanar waveguide.

The following geometric factor has been obtained from the recession of conducting walls of the coplanar strip shown in Fig. 3.3.

$$G = \frac{1}{\mu}\left[\left(-\frac{\partial L}{\partial t}+\frac{\partial L}{\partial h}\right)_{(1)}+\left(-\frac{\partial L}{\partial t}\right)_{(2)}+\left(-\frac{\partial L}{\partial W}\right)_{(3)}+\left(-\frac{\partial L}{\partial W}+2\frac{\partial L}{\partial S}\right)_{(4)}\right] \tag{3.19}$$

$$= \frac{4P'}{\pi S}\left(1+\frac{W}{S}\right)\frac{1+\frac{1.25}{\pi}\left[\frac{t}{W}+\ln\frac{4\pi W}{t}\right]}{\left[1+2\frac{W}{S}+\frac{1.25\,t}{\pi S}\left(1+\ln\frac{4\pi W}{t}\right)\right]^2} \tag{3.20}$$

where

$$P' = \left[\frac{K(k_e)}{K'(k_e)}\right]^2 P$$

and P is defined in previous section.

Chapter 4

Phenomenological Loss Equivalence Method for Quasi-TEM Transmission Lines with Thin Conductors

4.1. Introduction

For a planar quasi-TEM transmission line such as a microstrip line shown in Fig. 4.1(a), electromagnetic fields penetrate into the imperfect conductors while traveling along the axial direction. The field penetrations result in the resistance (R) and internal inductance (L_i) which are distributed in the axial direction in series to the external inductance (L) for ideal conductor. The distributed internal impedance ($Z_i = R + j\omega L_i$) makes the conductor loss and the dispersion of the transmission lines, which degrade the transmission characteristics. Therefore, the transmission lines must be characterized in a wide range of field penetration. Especially, a wideband transmission line using normal conductor must be analyzed in a wide penetration range since the penetration depth is proportional to the inverse square root of frequency.

If the penetration depth is very shallow compared to the conductor thickness, the surface current distribution will be the same as that of the ideal microstrip and then, we can apply the incremental inductance rule discussed in the previous section, to the structure. On the other hand, if the current completely penetrates into the conductor, the current distribution will be uniform inside the conductor and the distributed internal impedance can be readily calculated. Now, if the penetration is moderate, the current

distribution becomes nonuniform on the surface and almost exponentially decays from the surface into the conductor. Therefore, the incremental inductance method and the calculation at uniform distribution cannot be used for the moderate penetration.

In order to calculate the internal impedance of a transmission line, the current distribution must be known throughout the entire conductor. However, full-wave analysis and much of computation are needed in order to exactly calculate the whole current distribution. The idea of this phenomenological loss equivalence method is to phenomenologically transform a given quasi-TEM transmission line into an intermediate state of a single equivalent strip based on the discussion in the previous chapters and then, analyze the equivalent strip using the surface impedance for finite conductor thickness shown in (2.15).

4.2. Concept of the phenomenological equivalence

This method can be explained phenomenologically based on the geometric factor and the normal propagation of penetrated fields inside conductor discussed in Sections 3.3 and 2.2, respectively. For a given quasi-TEM line such as a microstrip line shown in Fig. 4.1(a), the conduction current is distributed just on the conductor surface at very shallow penetration. This is the case of a normal conductor at high frequencies or a superconductor of small penetration depth. Therefore, the conduction current can be said to be distributed just on entire circumference of the cross-sectional geometry. Since the internal regions of the conductor do not affect the field distributions at the shallow penetration, we can assume the conductors are hollow. This means the entire circumference can be unfolded and the nonuniform current distribution can be displayed in a straight line as shown in Fig. 4.1(b). Based on the

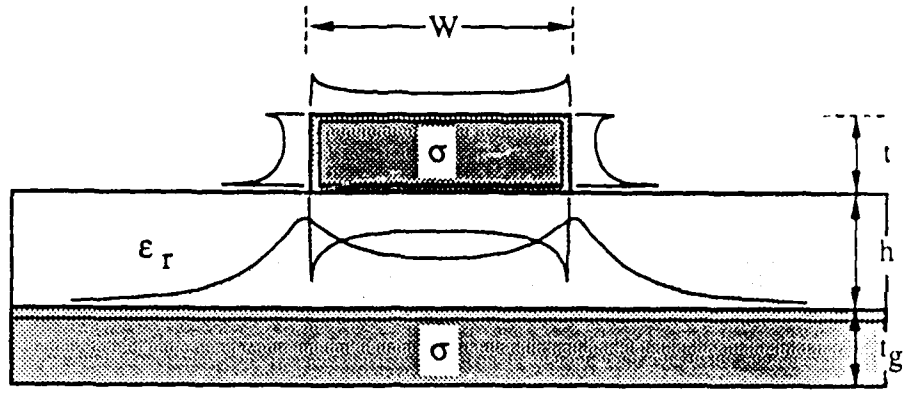

(a)

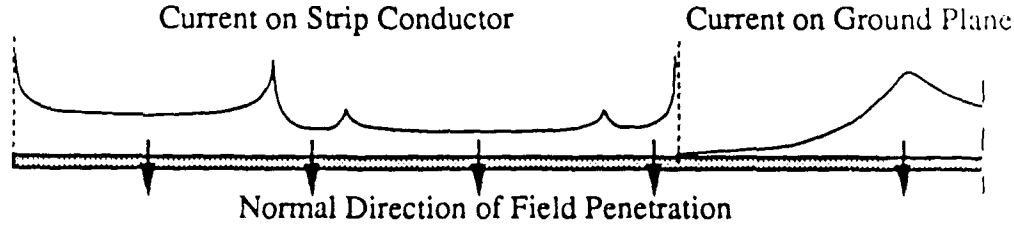

(b)

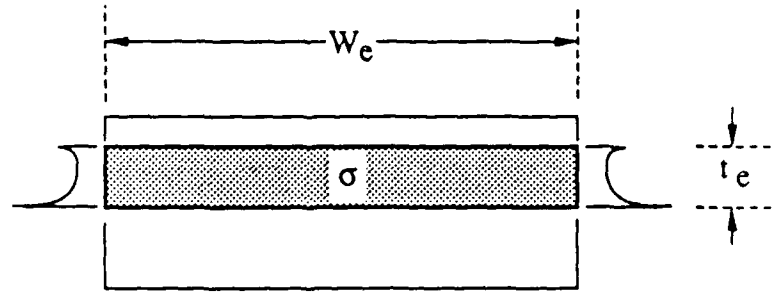

(c)

Fig. 4. 1. Cross-sectional geometries and current distributions of (a) a microstrip line, (b) the unfolded line, and (c) the equivalent strip

same geometric factor mentioned in the previous chapter, the nonuniform current distribution in the straight line can be represented effectively by a uniform current distribution on a single strip extended to an equivalent width (W_e) as shown in Fig.4.1(c).

Now, at deeper penetration shown using the current distribution of the microstrip in Fig. 4.1, the fields penetrate in normal direction from each conductor surface of the microstrip line. That is the normal direction in the unfolded straight line (vertical direction in Fig. 4.1(b)). The current penetrated inside the conductor therefore, can be displayed in the vertical direction. At the deep penetration, fields penetrated from one conductor face reach to the other face in normal direction and bounce back and forth between the two faces. Therefore, the field distribution between the two faces has almost the same form as that in a conducting plane with finite thickness shown in Section 2.3. Since the field distribution between every two-paired faces has the same form, the field distribution in the normal direction of the unfolded line can be described effectively by the field distribution inside an equivalent single strip with a finite thickness. Consequently, the given transmission line can be approximately transformed into the equivalent single strip having the equivalent width and thickness which are associated with the same geometric factor and the effective field distribution inside the conductors. Now, using the equivalent single strip of uniform surface current distribution, the internal impedance can be readily obtained and then, the propagation characteristics can be calculated from circuit model of the transmission line[20].

4.3. Equivalent single strip

In previous section, we introduced an equivalent single strip of the same internal impedance as the original transmission line through physical observation of the field penetration. The surface current on the equivalent strip is assumed to be uniform horizontally, but not vertically. The equivalent strip has the same conducting material as the original line while the width and thickness of the equivalent strip can be obtained independently of the conducting material used. The non-uniform distribution of the surface current of the transmission line is approximately expressed using the effective uniform current distribution on the equivalent width (W_e). The field distribution inside the conductor is also represented approximately using the effective thickness (t_e) of the equivalent strip. In order to obtain the width and the thickness of the equivalent strip, we consider the two completely different cases of shallow and complete penetrations.

4.3.1. Calculation of the equivalent width

First, the equivalent width (W_e) can be calculated, at a very shallow penetration, by equating the distributed internal impedance of the original line to that of the equivalent strip. In previous chapter, it is shown that the internal impedance of a transmission line can be calculated using the incremental inductance rule, if the penetration depth (δ, λ) into the conductor is very shallow compared to the conductor thickness (t), or $(\delta, \lambda) / t << 1$. Specifically, it is expressed as a simple form of $Z_i = Z_S G$ (Ω/m) as shown in (3.4), where Z_S is the surface impedance (Ω/square) of the conductor used and G is the geometric factor in dimension of m^{-1}. For instance, the Z_S is $(1+j)/\sigma\delta$ or $\sim 1/\sigma\lambda$ for normal conductors or superconductors, respectively. From the

incremental inductance rule, the G can be expressed in terms of the incremental inductance associated with the penetration of magnetic flux into the conductor as shown in (3.5). As an example, G ≈ 2/(strip width) for a very wide microstrip line[5]. The factor G depends only on the cross-sectional geometry of the transmission line with perfect conductor.

Under this condition of shallow field penetration, we also apply the incremental inductance rule to the equivalent strip. Since the current distribution is assumed to be uniform on the equivalent strip, the distributed internal impedance is just the surface impedance divided by the equivalent strip width. Then,

$$Z_i = Z_s / W_e \ (\Omega/m) \qquad (4.1)$$

where W_e is the equivalent width and Z_s is the surface impedance of the conductor used in the original line. Therefore, by equating (3.4) and (4.1), we can obtain the equivalent width at the shallow penetration as

$$W_e = 1 / G \ (m) \qquad (4.2)$$

The W_e obtained from the incremental inductance rule is only structure-dependent and free from the conducting material used.

4.3.2. Calculation of the equivalent thickness

Now, if the field penetrates deep into the conductor, the distributed internal impedance will also depend on the strip thickness. However, if the current distribution on the surface of the transmission line can be assumed to be almost unchanged, e.g., in the case of quasi-TEM transmission line, we can still use the equivalent width (W_e) calculated above and include the field penetration effect into the conductor thickness (t_e)

of the equivalent strip. The equivalent thickness (t_e) can be obtained by equating both internal impedances in the case of uniform current distribution at complete penetration. At the uniform distribution of current, the distributed internal impedance of the original line can be simply expressed as

$$Z_i = 1/(\sigma A) \tag{4.3}$$

where A is the effective cross-section of the original structure at the uniform current distribution. For instance, A is just the cross-section (Wt) of the microstrip conductor because of the infinite ground plane. At the same complete penetration, the equivalent strip has the internal impedance as follows

$$Z_i = 1/(\sigma W_e t_e) \tag{4.4}$$

Then, using (4.3) and (4.4), we can find the equivalent thickness (t_e) as

$$t_e = A/W_e = AG \tag{4.5}$$

Here, W_e and t_e depend only on the cross-sectional geometry of the original transmission line since G and A can be calculated from the cross-sectional geometry. Therefore, an equivalent strip obtained from a given geometry of the transmission line can be used approximately for any conducting material and the penetration depth by simply substituting the strip material.

4.4. Calculation of the distributed internal impedance at any penetration

Now, using the equivalent strip obtained from the cross-sectional geometry, and the conductivity of a given transmission line, we can calculate the overall distributed internal impedance at any field penetration. For the equivalent strip with the laterally uniform current distribution, the overall distributed internal impedance can be

calculated using the equivalent strip width (W_e) and the surface impedance (Z_s^t) of a flat plane conductor with finite thickness shown in (2.15). The surface impedance can be explained based on the total longitudinal current and the longitudinal electric field on the strip surface. The longitudinal current distribution in the vertical direction of the strip is subject to the boundary conditions at the two strip surfaces. From these conditions, the longitudinal current (I) integrated through the strip thickness can be obtained in terms of the longitudinal electric field (E_0) on the strip surface. Therefore, the ratio (E_0/I) becomes the surface impedance (Z_s^t) in (2.15).

Since the laterally uniform current of the equivalent strip extends over the finite width W_e (= 1/G), the distributed internal impedance (Z_i) of the equivalent strip becomes Z_s^t/W_e (= Z_s^t G) by replacing the surface impedance in (4.1) with (2.15). Finally, for a planar quasi-TEM transmission line with finite conductor thickness, the distributed internal impedance at any field penetration can be approximately calculated through the equivalent strip as

$$Z_i = R + j\omega L_i = Z_s^t / W_e = Z_s G \coth [\, t G A \,] \quad (\Omega/m) \qquad (4.6)$$

The usefulness of this method comes from very simple calculations of G and A used in (4.6). Here, G and A of a transmission line can be calculated using the empirical formulas and from the actual cross-section of the line, respectively. Also, Z_s and t can be easily obtained from the conductivity of the conducting material used. Therefore, all the calculations consist only of simple calculations of several formulas. This method can also be applied to many quasi-TEM transmission lines, i.e., microstrip, coplanar waveguide, coplanar strip, and so forth.

4.5. Calculation of the propagation characteristics

Propagation characteristics (i.e. attenuation, effective index, and characteristic impedance) of the original transmission line can be readily calculated from a circuit model of transmission line[20] shown in Fig. 4.2. In the model, the distributed resistance (R) and internal inductance (L_i) calculated from (4.6) are added in series to the external inductance (L_o) of the transmission line, while the shunt capacitance (C) almost remains constant for the field penetration. The conductance due to the dielectric loss is also incorporated through the calculation of effective loss tangent[6],[21]. Then, we can use general formulas of the circuit model to calculate the propagation characteristics.

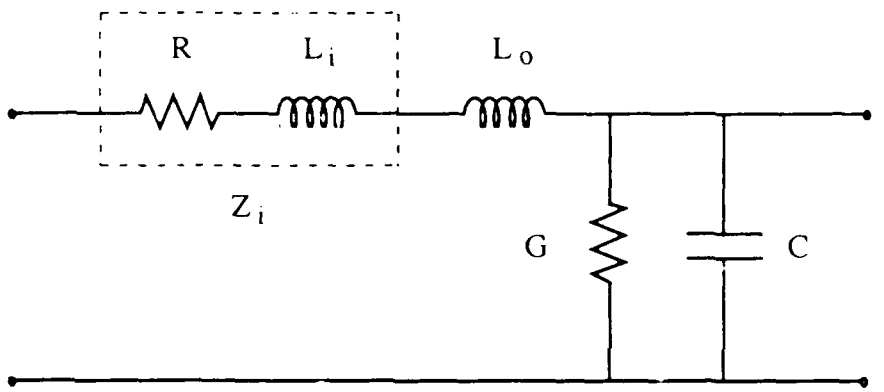

Fig. 4. 2. Circuit model of a transmission line including the internal impedance due to field penetration

Chapter 5

Calculated Results for Normal-state and Superconducting Microstrip Lines and a Normal-state Coplanar Waveguide

5.1. Introduction

In order to verify the proposed phenomenological loss equivalence method, the method is applied to microstrip lines using a copper conductor and a high-T_c superconductor and compared the calculated data with published data. Since there is no published data on thin coplanar waveguide and coplanar strip at deep penetration, another comparison is performed with experimental data measured for very thin coplanar waveguide. Through the comparisons in the wide ranges of frequency and geometrical dimensions, we confirmed the proposed phenomenological loss equivalence method is valid and very accurate for quasi-TEM transmission lines in a wide range of field penetration.

5.2. Calculated results for a copper microstrip at 77 K

For the copper microstrip line shown in Fig.5.1, many transmission characteristics were calculated using the phenomenological loss equivalence method (PEM) in a wide frequency range and for a wide range of geometrical dimensions. In Fig.5.2, the results are compared with the published data calculated by the finite element method (FEM)[5].

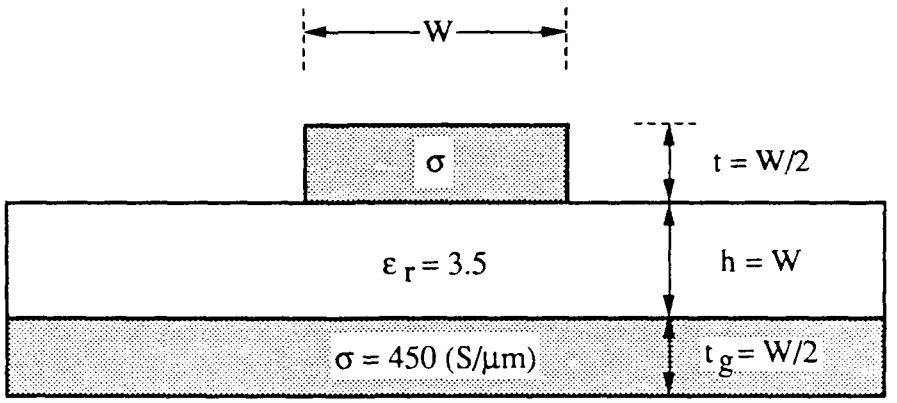

Fig. 5. 1. Copper microstrip line at 77 K with different strip widths (2, 5, and 10 μm)

One set of the PEM data (PEM-1 in Fig. 5.2) are calculated by directly applying the method to the microstrip based on the geometric factor derived in Section 3.4.1. Note that the microstrip used in the FEM analysis[5] has the strip conductor embedded in the infinitely thick dielectric polyimide, while in this PEM calculation we consider a real situation of the strip conductor lying just on top of the finite dielectric. Therefore, the phase velocities of the FEM data at high frequency approach the velocity of light in the dielectric medium and are higher than those calculated from the empirical formulas. In order to compare the PEM data with the FEM data in a same situation and verify the PEM itself, another set of PEM data (PEM-2 in Fig. 5.2) was generated based on the effective indices mentioned above.

As shown in Fig. 5.2, all the PEM data of the second set are in excellent agreement with the FEM data in wide ranges of frequency and geometrical dimension.

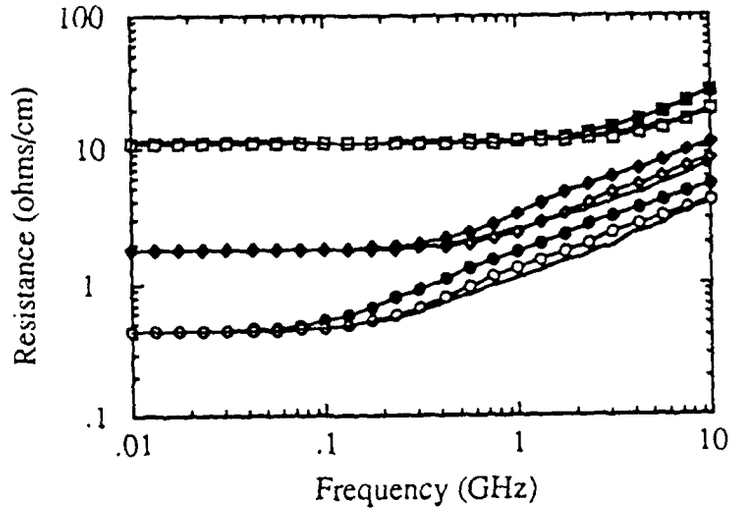
100
10
1
.1
Resistance (ohms/cm)
.01
.1
1
10
Frequency (GHz)

(a)

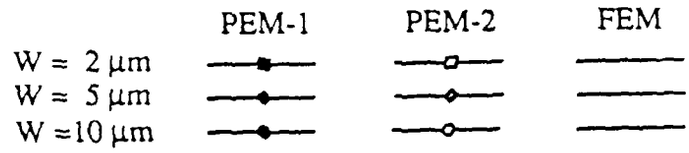
PEM-1
PEM-2
FEM
W = 2 μm
W = 5 μm
W =10 μm

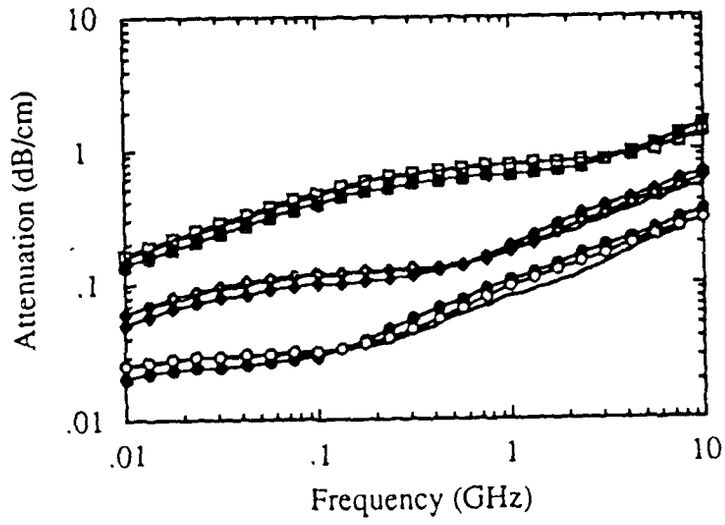
10
1
.1
.01
Attenuation (dB/cm)
.01
.1
1
10
Frequency (GHz)

(b)

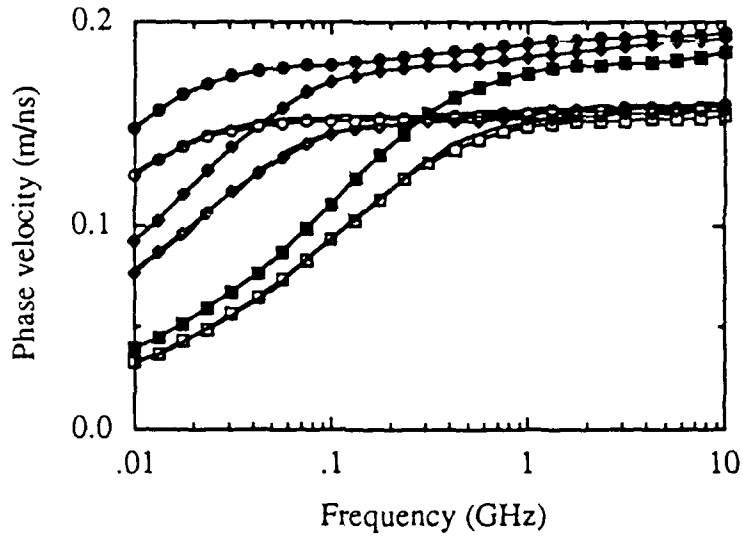
0.2
0.1
0.0
Phase velocity (m/ns)
.01
.1
1
10
Frequency (GHz)

(c)

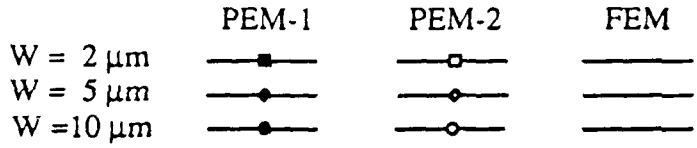
PEM-1
PEM-2
FEM
W = 2 μm
W = 5 μm
W =10 μm

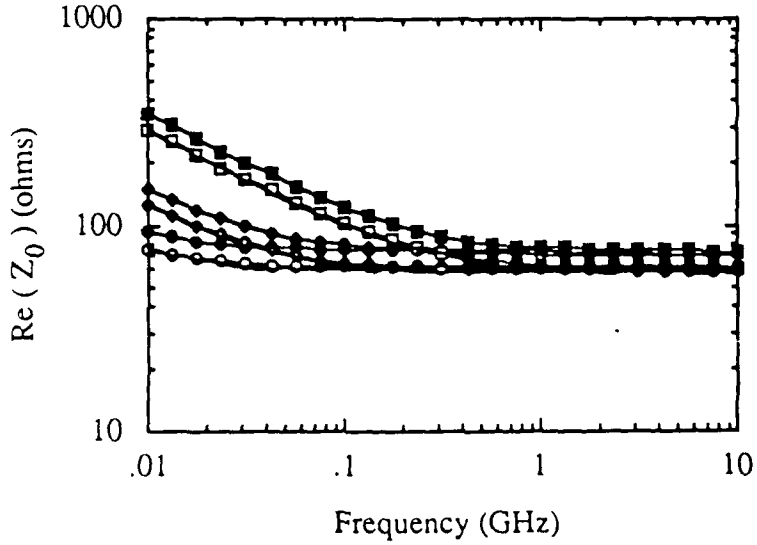
1000
100
10
Re (Z_0) (ohms)
.01
.1
1
10
Frequency (GHz)

(d)

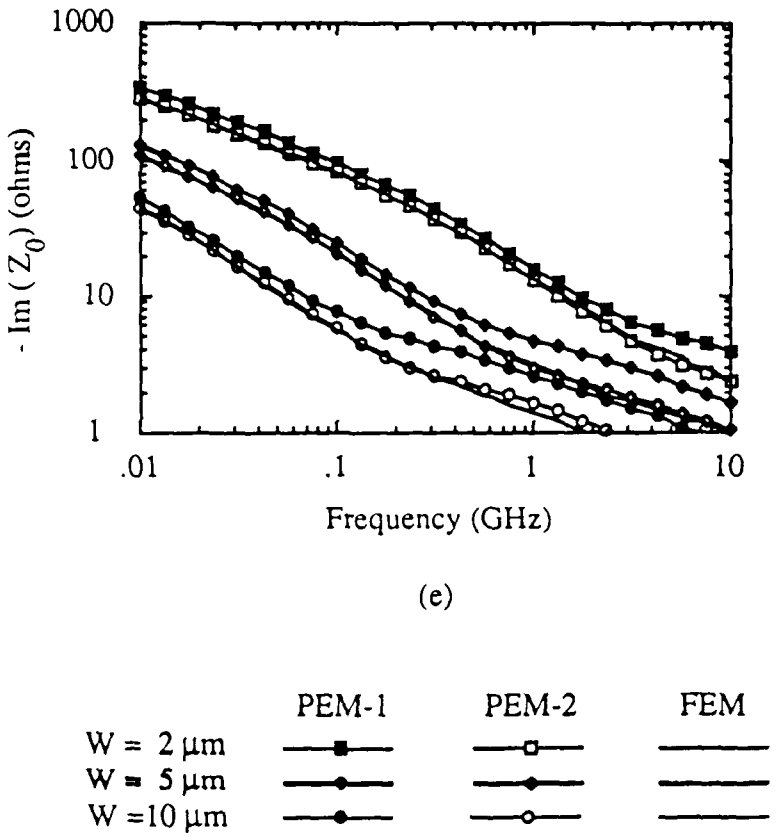

Fig. 5. 2. (a) Distributed resistance, (b) Attenuation, (c) Phase velocity, (d) Real and (e) Imaginary parts of the characteristic impedance of the copper microstrip line, shown in Fig. 5. 1, for different strip widths at 77K. PEM-1 and PEM-2 show PEM data calculated respectively using the empirical formulas, and the geometric factors and effective indices obtained from the FEM data at high frequency.

All of the PEM-1 data agree well with the FEM data except the effective indices due to the different dielectric thicknesses considered. This indicates the validity of the PEM for the characterization of quasi-TEM transmission lines in a wide range of field penetration.

There are two deflection points for each attenuation curve shown in Fig. 5.2(b). The deflection at upper frequency is associated with the saturation of the field penetration due to the finite strip thickness. Another deflection comes out at the lower frequency where the total reactance($j \omega [L + L_i]$) and the resistance (R) become about the same. A wide and flat attenuation region is in between the two frequencies and can be shifted to the lower frequency by increasing the conductivity or the cross-section of the line. These deflection points will exist in all planar quasi-TEM transmission lines with normal conductors.

5.3. Calculated results for a superconducting microstrip line

A thin microstrip line having the geometry of Fig. 5.3 is chosen for an application of the PEM to superconducting line. In reference [22], the Monte-Carlo method (M.C.) is used to analyze the microstrip line with aluminum or high-T_c superconductor (Ba-Y-Cu-O). The high-T_c superconductor is described using the two-fluid model in both this PEM and the M.C., although the validity of this model in high-T_c material is uncertain. It is used here only to make a comparison of the PEM data with the M.C. data.

Using the PEM, the attenuations and the phase velocities are calculated and compared with the data from the M.C. method in Fig.5.4. They are in very good agreement in a wide range of frequency and show the validity of the PEM for a

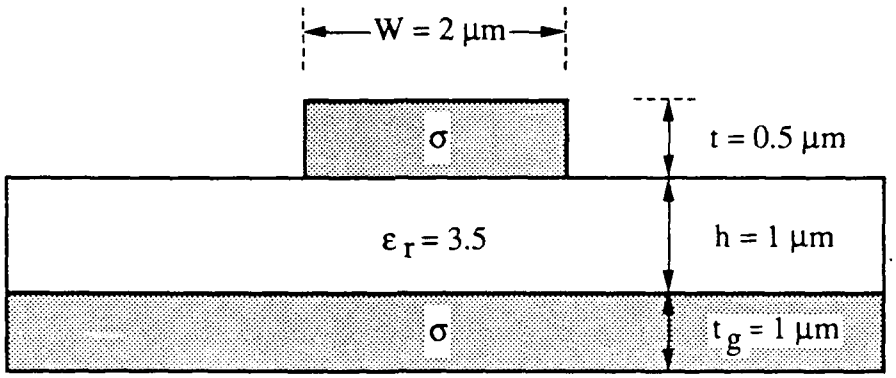

High-T_c superconductor (Ba-Y-Cu-O) : $T_c = 92.5$ (K), $\lambda_0 = 0.14$ (μm), σ_n at $T_c = 0.5$ (S/μm)

or Aluminum : σ at 77 K = 150 (S/μm)

Fig. 5. 3. Microstrip line using high-T_c superconductor or aluminum

superconducting line. The superconducting line shows very small attenuation and virtually non-dispersive transmission, while the aluminum line is very lossy at high frequency and dispersive in low frequency region. Although the superconducting line has the attenuation proportional to the square of frequency, it is almost ideal for transmission except at very high frequency close to the bandgap frequency.

Since the penetration depth of the superconductor at 77K (=0.2μm) is not so deep compared to the microstrip thickness (=0.5μm), the penetration effect cannot be seen clearly in this geometry. The penetration effect rather can be seen clearly in the aluminum line as well as in the previous copper line, because their skin depths are frequency-dependent and hence, very deep at low frequency. Therefore, the PEM will

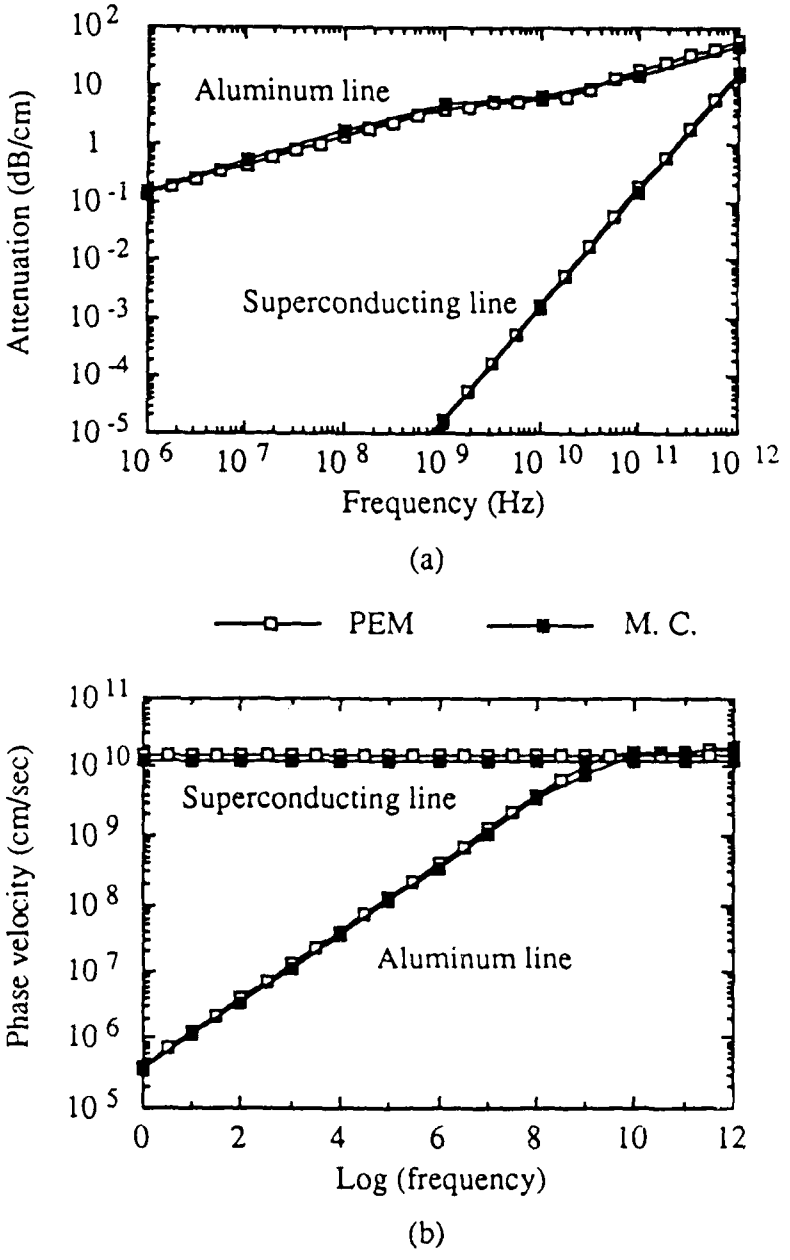

Fig. 5. 4. (a) Attenuation and (b) Phase velocity of the superconducting and aluminum microstrip lines at 77K shown in Fig. 5. 3.

be more effective for very thin and narrow superconducting lines. For those small lines, the line thicknesses are not thick enough to apply the incremental inductance method and a simple modification of the surface impedance[1],[23],[24] will be inaccurate due to the lateral surface current spreading at very deep field penetration.

5.4. Calculated results for a thin coplanar waveguide

In order to compare PEM data with experimental data for coplanar waveguide, we have applied the PEM to the thin coplanar waveguide shown in Fig. 5.5. The PEM data are obtained using the geometric factor in equation (3.16) and the internal impedance in equation (4.6). The thin (1.25 μm) coplanar waveguide is on a very thick (1270 μm) quartz substrate in which the dielectric loss and the thickness effect are negligible. Total length of the coplanar waveguide is 9.5 mm (one end is shorted using silver paste and S_{11} is measured through the other end). Since silver is used for the conductor, the skin depth is about 2 μm at 1 GHz. Therefore, the field penetration effect can be seen clearly in a wide frequency range of the measured data (from 1 to 40 GHz).

As shown in Fig.5.6(a), the PEM data are very close to the measured data in the wide frequency range. This means the PEM is valid for a coplanar waveguide in wide range of field penetration because the skin depth depends on the frequency. A slight deviation from the measured data at lower frequency is considered due to calibration errors or the inaccurate thickness and conductivity used for the PEM calculation. Radiation and substrate mode generation at input discontinuity can also result in the slight deviations at dips in Fig.5.6(a). Calculated distributed resistance and conductor loss are shown in Fig.5.6(b) in which the resistance and the attenuation become

saturate below 10 GHz. At the frequency the skin depth is about half of the conductor thickness and the penetration effect becomes important. Although the calculated data are not shown below 1 GHz, the flat attenuation zone mentioned in Section 5.2 also exists around 1 GHz in this coplanar waveguide.

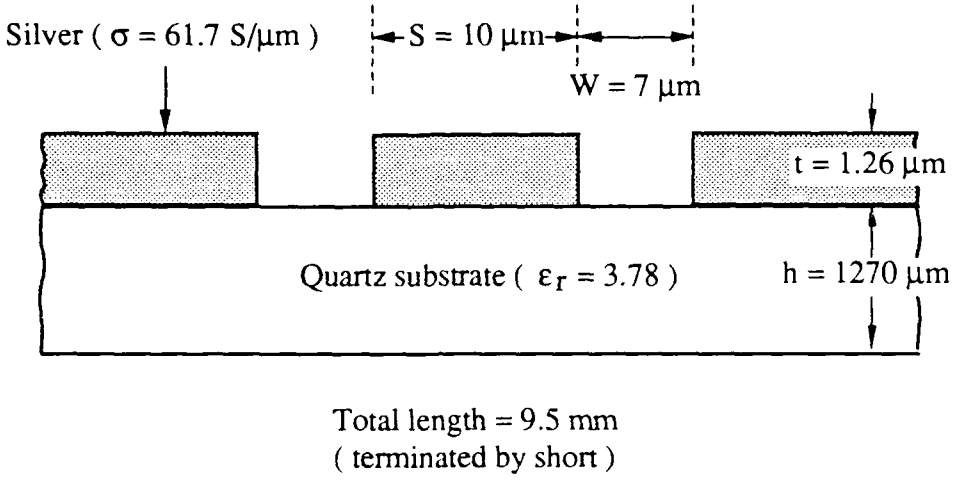

Fig. 5. 5. Thin coplanar waveguide on a quartz substrate

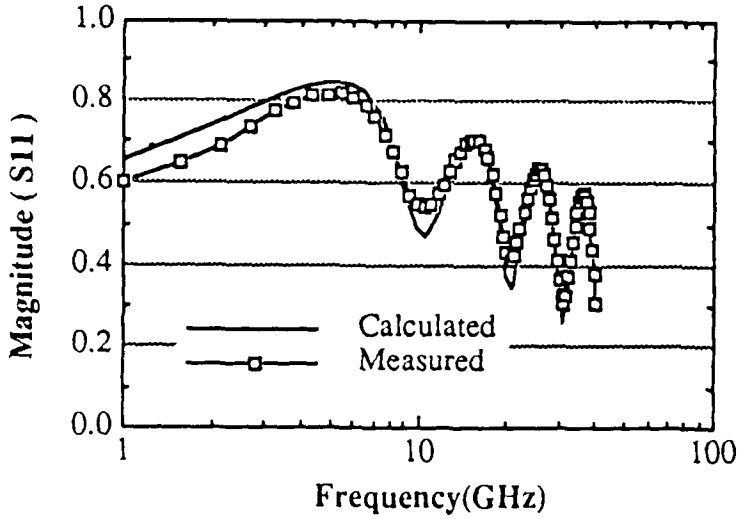

(a)

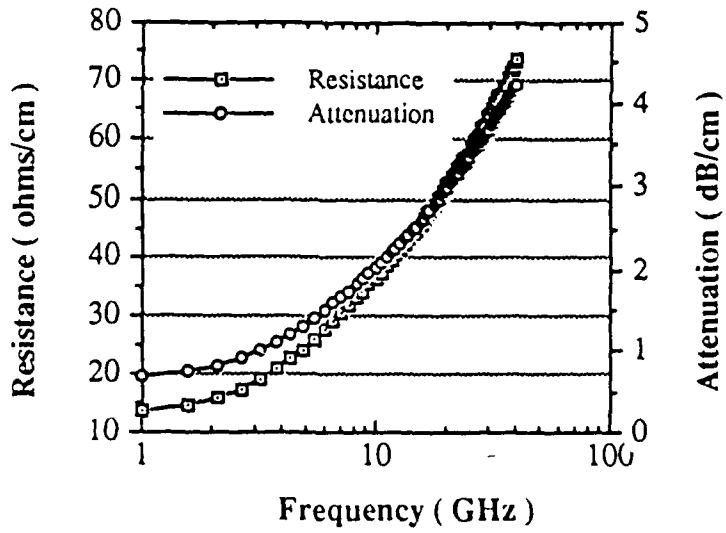

(b)

Fig. 5. 6. (a) S_{11} and (b) Distributed resistance and attenuation of the coplanar waveguide with short termination shown in Fig. 5.5.

Chapter 6

Conclusion

For very thin normal-state or superconducting transmission line, conductor loss must be characterized in a wide field-penetration range by taking the field penetration effect into consideration. Full-wave analyses of the conductor loss however, are not appropriate for computer-aided-design implementation since they require extensive formulations and numerical computations in order to consider the field penetration effect.

A phenomenological loss equivalence method is proposed to characterize the conductor loss of a planar quasi-TEM transmission line made of a normal or superconductor in a wide range of field penetration. This phenomenological loss equivalence method is based on the observation of the current distribution changing as the quasi-static field of a quasi-TEM transmission line penetrates more into the conductor. In this method, a planar quasi-TEM transmission line, having a finite conductor thickness on the order of the penetration depth, is approximated by an equivalent single strip which has the same conductor loss as the transmission line. The geometry of the equivalent strip is obtained only from the cross-sectional geometry of the original line, while the conducting material is the same as that of the original line. Since the geometry of the equivalent strip obtained is material-independent, it can be used for any normal-state or superconducting line by substituting the conducting material. Therefore, the distributed

internal impedance of the transmission line can be approximately calculated from the equivalent single strip and all the propagation characteristics can be obtained by incorporating the internal impedance into the circuit model of the transmission line.

In order to verify the method, we applied the method to microstrip lines made of thin copper and high-T_c superconductor as well as a coplanar waveguide made of silver. The calculated PEM data show very good agreement with published data (by Finite Element Method and Monte-Carlo Method) and experimental data in wide ranges of field penetration and geometrical dimensions. Since the method consists of simple calculations of several formulas obtained through physical observation of field penetration, it can be readily applied to the computer-aided-design implementation.

References

[1] R. L. Kautz, " Miniaturization of normal-state and superconducting striplines," J. Res. Nat. Beau. Stand., Vol. 84, pp. 247-259, 1979.

[2] H. A. Wheeler, " Formulas for the skin effect," Proc. IRE, Vol. 30, pp. 412-442, September 1942.

[3] P. Waldow and I. Woff, " The skin-effect at high frequencies," IEEE Trans. Microwave Theory Tech., Vol. MTT-33, pp. 1076-1081, October 1985.

[4] G. Costache," Finite element method applied to skin-effect problems in strip transmission lines," IEEE Trans. Microwave Theory Tech., Vol. MTT-35, pp. 1009-1013, November 1987.

[5] U. Ghoshal and L. Smith, " Skin effects in narrow copper microstrip at 77 K," IEEE Trans. Microwave Theory Tech., Vol. MTT-36, pp. 1788-1795, December 1988.

[6] J. D. Welch and H. J. Pratt, " Losses in microstrip transmission systems for integrated microwave circuits," NEREM Record, pp. 100-101, November 1966.

[7] H.-Y. Lee and T. Itoh, " Phenomenological loss equivalence method for planar quasi-TEM transmission line with a thin normal conductor or superconductor, "

IEEE Trans. Microwave Theory Tech., Vol. MTT-37, Number 12, December 1989.

[8] H.-Y. Lee and T. Itoh, " Wideband conductor loss calculation of planar quasi-TEM transmission lines with thin conductors using a phenomenological loss equivalence method," IEEE International Microwave Symposium, Long Beach, California, pp. 367-370, June 1989.

[9] H.-Y. Lee, K.-S. Kong, T. Itoh, " Conductor loss calculation of superconducting microstrip line using a phenomenological loss equivalence method," 19th European Microwave Conference, London, England, September 1989.

[10] M. Tinkham, Superconductivity, Gordon and Breach, New York (1965).

[11] D. C. Mattis and J. Bardeen, " Theory of the anomalous skin effect for normal and superconducting metals," Phys. Rev., Vol.-111, pp. 412-417, July 1958.

[12] A. B. Pippard, " Metallic conduction at high frequencies and low temperatures," in Advances in Electronics and Electron Physics, Vol.-VI, L. Marton Ed., New York (1954), pp. 1-16.

[13] R. A. Pucel et. al., " Losses in microstrip," IEEE Trans. Microwave Theory Tech., Vol. MTT-16, pp. 342-350, October 1968 (see also correction in MTT-16, pp. 1064).

[14] K. C. Gupta, R. Garg, and I. J. Bahl, Microstrip lines and slotlines, Artech House, Inc., (1979).

[15] I. J. Bahl and R. Garg, " Simple and accurate formulas for a microstrip with finite strip thickness," Proc. IEEE, Vol. 65, pp. 1611-1612, November 1977.

[16] E. Hammerstadt and O. Jensen, " Accurate models for microstrip computer-aided design," 1980 IEEE International Microwave Symposium Digest, pp. 407-409, June 1980.

[17] C. P. Wen, " Coplanar waveguide : A surface strip transmission line suitable for non-reciprocal gyromagnetic device application," IEEE Trans. Microwave Theory Tech., Vol. MTT-17, pp. 1087-1090, 1969.

[18] M. E. Davis et. al., " Finite-boundary corrections to the coplanar waveguide analysis," IEEE Trans. Microwave Theory Tech., Vol. MTT-21, pp. 594-596, 1973.

[19] W. Hilberg, " From approximations to exact relations for characteristic impedances," IEEE Trans. Microwave Theory Tech., Vol. MTT-17, pp. 259-265, 1969

[20] S. Ramo, J. R. Whinnery, and T. Van Duzer, Fields and Waves in Communication Electronics, John Wiley and Sons, Inc., New York (1965).

[21] M. V. Schneider, " Dielectric loss in integrated microwave circuits," Bell Sysm. Tech. J., Vol. 48, pp. 2325-2332, 1969.

[22] O.K. Kwon, B.W. Langley, R.F.W. Pease, and M.R. Beasley, " Superconductors as very high-speed system-level interconnects", IEEE Electron Device Letters, Vol. EDL-8, pp. 582-585, December 1987

[23] R. L. Kautz, " Picosecond pulses on superconducting striplines," J. Appl. Phys., Vol. 49, pp. 308-314, 1978.

[24] J. F. Whitaker, R. Sobolewski, D. R. Dykaar and T. Y. Hsiang," Propagation model for ultrafast signals on superconducting dispersive striplines", IEEE Trans. Microwave Theory Tech., Vol. MTT-36, pp. 277-285, February 1988.